PATTERN FORMATION ANALYSIS IN THE SCHNAKENBERG MODEL

CASPER H. L. BEENTJES

Mathematical Institute, University of Oxford, Oxford, UK

Abstract. Literature suggests that steady chemical patterns could serve as an explanation for pattern formation in biology [17]. One way to generate these spatial patterns is by the Turing instability in reaction-diffusion equations [15]. In this report we explain some of the theory of the Turing instability with a focus on a prototype model by Schnakenberg [13]. The parameter values that allow for pattern formation are investigated in more detail. Numerical explorations using an IMEX-pseudospectral method [12],[14] are made to test predictions for the one-dimensional Schnakenberg model.

1. Introduction

The self-emergence of order out of a seemingly disordered situation has inspired scientific study for many years and in many different fields such as physics, chemistry, ecology and biology. One of these fields which displays a wide variety of self-organisation is developmental biology, which tries to unravel among others pattern formation on animal coats (e.g. leopard's spots, zebra's stripes), butterfly wings and the evolution of vertebrate limbs. In this study of the origin of shape and form, *morphogenesis*, one of the possible proposed ways to create structure is the theory of positional information by Wolpert [17]. It assumes that cells differentiate according to their position in space. To the cells' positions different positional values can be attributed, such as the time cells spend in a certain area or the presence of a chemical, which is called a morphogen in this context. In the case of a morphogen there can be different proposals as to how this differentiates the cells, such as based on the gradient of the morphogen's concentration or its actual concentration. One can say that the way the cells differentiate is encoded in a pre-pattern, constructed by a distribution of chemicals. This paper focusses on establishing such a pre-pattern of morphogens by means of reaction-diffusion equations. This approach has been put forward by Alan Turing in his seminal paper [15] which was ahead of its time.

The main revelation Turing described was diffusion-driven instability resulting in heterogeneous patterns, which, in some sense, almost seems counter-intuitive. Normally diffusion tends to spread out concentrations as to create a homogeneous distribution and not a spatially heterogeneous mixture. It is the interplay of at least two different chemicals which can result in spatial pre-patterns as he showed, thereby initiating a new branch in the mathematical field of reaction-diffusion systems, pattern formation.

This paper studies the behaviour of chemical reaction models giving rise to these so-called Turing patterns. More specifically it analyses the Schnakenberg model [13]. Although the Schnakenberg model is one of many different reaction models which exhibit Turing pattern formation, and is in some sense a hypothetical model, it stands out from the other ones as a good prototype model

E-mail address: beentjes@maths.ox.ac.uk.

Date: Michaelmas term 2014.

2010 *Mathematics Subject Classification.* 35B36,92-08,92B05.

This text is based on a technical report for the Michaelmas 2014 Oxford Mathematics course B5.5 Mathematical Biology & Ecology lectured by Prof. P. Maini.

because of its simplicity. This allows us to make some analytical progress in the first part of this paper, which is devoted to a (semi-)analytical treatment of Turing-pattern formation, whereas the last chapter explores the Schnakenberg model numerically to provide tests for the earlier derived theory.

1.1. **Schnakenberg model.** Most of the study of Turing patterns is done on chemical reaction-diffusion systems. These are derived by making a model for the chemical reactions and deriving from this a set of (partial) differential equations describing the evolution of the concentration of chemicals. Schnakenberg developed his kinematic reaction model [13] in search for a minimal, but still chemically sensible model exhibiting so-called limit-cycle behaviour, i.e. temporal periodic solutions. Minimal in the sense that it invoked a minimal number of reactions and reactants. Inspiration for such an idea came from research in different biological areas such as ecological cycles of population densities and metabolic regulation, both showing time-dependent behaviour. He showed that such a model would need to involve at least three reactions of which one needs to be an autocatalytic reaction. For general chemicals X, A, B and Y he derived the following reaction scheme

$$X \underset{k_{-1}}{\overset{k_1}{\rightleftharpoons}} A, \qquad B \xrightarrow{k_2} Y, \qquad 2X + Y \xrightarrow{k_3} 3X. \tag{1}$$

By setting $\alpha = [A]$, the concentration of A, and $\beta = [B]$, $\Upsilon = [Y]$ and $\chi = [X]$ we derive, using the law of mass action, a system of ordinary differential equations (ODEs)

$$\frac{d\chi}{dt} = k_{-1}\alpha - k_1\chi + k_3\chi^2\Upsilon, \tag{2}$$

$$\frac{d\Upsilon}{dt} = k_2\beta - k_3\chi^2\Upsilon, \tag{3}$$

$$\frac{d\alpha}{dt} = k_1\chi - k_{-1}\alpha, \tag{4}$$

$$\frac{d\beta}{dt} = -k_2\beta, \tag{5}$$

describing the temporal evolution of the reactants' concentrations. Now the assumption is made that α, β are roughly constant, e.g. the reactions are performed in an environment where there is an abundance of A, B. The system then simplifies to a coupled (non-linear) system for χ, Υ (2),(3) in which α, β are now assumed to be positive constants. This system of equations allows for the existence of limit-cycles as was shown by Schakenberg. Next one can introduce a spatial dependency of the concentrations and encompass for the movement of chemicals by adding diffusion. Remarkably doing so we end up with a minimal, or at least algebraically simple, system which can give rise to Turing patterns. The resulting partial differential equation (PDE) system is given by

$$\frac{\partial\chi}{\partial t} = d_\chi\nabla^2\chi + k_{-1}\alpha - k_1\chi + k_3\chi^2\Upsilon, \tag{6}$$

$$\frac{\partial\Upsilon}{\partial t} = d_\Upsilon\nabla^2\Upsilon + k_2\beta - k_3\chi^2\Upsilon. \tag{7}$$

The above can be written in the general framework of a reaction-diffusion system

$$\frac{\partial\mathbf{c}}{\partial t} = D\nabla^2\mathbf{c} + \mathbf{f}(\mathbf{c}), \tag{8}$$

where $\mathbf{c}$ denotes a vector of chemical concentrations, D a matrix containing the positive diffusion coefficients (diagonal in the case of the Schnakenberg model) and $\mathbf{f}$ a vector containing reaction terms, which are likely to be non-linear.

In order to analyse the model in more detail we carry out a non-dimensionalisation to reduce the model to a simpler formulation, containing fewer free parameters. We set

$$u = \chi\sqrt{\frac{k_3}{k_1}}, \quad v = \Upsilon\sqrt{\frac{k_3}{k_1}}, \quad a = \frac{k_{-1}\alpha}{k_1}\sqrt{\frac{k_3}{k_1}}, \quad b = \frac{k_2\beta}{k_1}\sqrt{\frac{k_3}{k_1}}, \tag{9}$$

$$d = \frac{d_\chi}{d_\Upsilon}, \qquad \gamma = \frac{L^2 k_1}{d_\chi}, \qquad \hat{t} = \frac{d_\chi t}{L^2}, \qquad \hat{\mathbf{x}} = \frac{\mathbf{x}}{L}. \tag{10}$$

By substitution of these dimensionless parameters and by omission of the hats for simplicity of notation, we arrive at the dimensionless Schnakenberg model involving the 4 positive parameters a, b, γ and d

$$\frac{\partial u}{\partial t} = \nabla^2 u + \gamma(a - u + u^2 v) = \nabla^2 u + \gamma f(u, v), \tag{11}$$

$$\frac{\partial v}{\partial t} = d\nabla^2 v + \gamma(b - u^2 v) \qquad = d\nabla^2 v + \gamma g(u, v). \tag{12}$$

Following this procedure, more general reaction diffusion systems can be derived from a different set of chemical reactions. A few well-known examples are the Gray-Scott model [7], Gierer-Meinhardt model [6] and the FitzHugh-Nagumo model [5], all resulting in non-linear $f(u, v)$ and $g(u, v)$ of a higher algebraic complexity. It is for the ease and clearness of presentation that this paper is therefore mostly concerned with the Schnakenberg model, although all the described procedures can equally well be applied to other models.

2. Turing pattern formation

Before starting the analysis of the Schnakenberg model, we place a short note on the biological/chemical constraints posed on this model. Since the model tries to describe the evolution of concentrations of chemicals it makes only sense to have positive u, v. The parameters a, b, γ, d must be positive as well to make physically sense. Of course it is possible to study the system without these constraints by using purely mathematical arguments, but the aim of this paper is to stick to the biologically sensible regions of the model.

In order to analyse the reaction-diffusion models they need to be supplied with initial conditions and boundary conditions to make the problem well-posed. In this paper we take homogeneous Neumann boundary conditions, i.e.

$$(\mathbf{n} \cdot \nabla)\mathbf{c} = 0, \qquad \text{on } \partial\Omega, \tag{13}$$

where $\partial\Omega$ is the edge of the domain Ω on which we solve the problem. These boundary conditions are chosen because we are interested in self-organisation of patterns and thus an isolated system without external influence, which is ensured by Neumann boundary conditions. We also assume initial conditions are provided, i.e. $\mathbf{c}(\mathbf{x}, 0)$ is given.

A good starting point in analysing a system of equations like (11,12) is to look for a homogeneous steady state solution, i.e. a state where all spatial and temporal derivatives vanish, and thus to look for solutions to $f(u, v) = g(u, v) = 0$. In case of the Schnakenberg model only one such state can be found

$$u^* = a + b, \quad v^* = \frac{b}{(a + b)^2}. \tag{14}$$

Note that both are positive numbers and are thus in our allowed solution space. The crucial idea of Turing was that it is possible to have such steady states which are stable in the absence of diffusion, but which turn unstable in the presence of diffusion and form spatially heterogeneous patterns, hence the name diffusion-driven instability or Turing pattern formation. The next question then is, under what conditions can we observe Turing patterns? To answer this question we will derive the so-called Turing conditions closely following Murray [10].

2.1. **Turing conditions.**

2.1.1. *Stability in absence of diffusion.* In the absence of diffusion the model takes the form of a system of ODEs

$$\frac{du}{dt} = \gamma f(u,v), \tag{15}$$

$$\frac{dv}{dt} = \gamma g(u,v). \tag{16}$$

To look at the stability of the steady state u^*, v^* we perform a linear stability analysis. We perturb the steady state by a small perturbation, i.e. $u = u^* + \tilde{u}$ and $v = v^* + \tilde{v}$, where the perturbations are such that $|\tilde{u}|, |\tilde{v}| \ll 1$. The growth of these perturbations determines the stability. The result is a linearised system of equations around the steady state

$$\frac{d\tilde{\mathbf{u}}}{dt} = \gamma \begin{pmatrix} f_u & f_v \\ g_u & g_v \end{pmatrix}_{(u^*,v^*)} \tilde{\mathbf{u}} = \gamma J_{(u^*,v^*)} \tilde{\mathbf{u}}, \qquad \tilde{\mathbf{u}} = \begin{pmatrix} \tilde{u} \\ \tilde{v} \end{pmatrix}, \tag{17}$$

where the subscripts denote partial derivatives and the Jacobian J is evaluated at the steady state $\mathbf{u^*} = (u^*, v^*)^T$. The solution to this system is known to be given by

$$\tilde{\mathbf{u}} = \mathbf{a} e^{\lambda_+ t} + \mathbf{b} e^{\lambda_- t}, \tag{18}$$

in the situation where λ_+, λ_- are the distinct eigenvalues of the Jacobian evaluated at the steady state. In order to have stability it is necessary for the perturbations not to grow in time and thus the eigenvalues must have real part less than zero, i.e. $\Re(\lambda_+) < 0, \Re(\lambda_-) < 0$. The eigenvalues of a 2×2-matrix can be written in terms of its trace $\mathcal{T} = \mathrm{Tr}(J)$ and determinant $\mathcal{D} = \det(J)$

$$\lambda_\pm = \frac{\gamma}{2}\left(\mathcal{T} \pm \sqrt{\mathcal{T}^2 - 4\mathcal{D}}\right). \tag{19}$$

The condition on stability then transforms to two conditions

(i) $\mathcal{T} < 0 \implies f_u + g_v < 0$,
(ii) $\mathcal{D} > 0 \implies f_u g_v - f_v g_u > 0$,

where all the expressions have to be evaluated at the steady state.

2.1.2. *Diffusion driven instability.* Now we turn on the diffusion and look again for the stability of the system using the same perturbation procedure, only now arriving at a different linearised system

$$\frac{\partial \tilde{\mathbf{u}}}{\partial t} = \left(\begin{pmatrix} 1 & 0 \\ 0 & d \end{pmatrix} \nabla^2 + \gamma \begin{pmatrix} f_u & f_v \\ g_u & g_v \end{pmatrix}_{(u^*,v^*)} \right) \tilde{\mathbf{u}} = \left(D\nabla^2 + \gamma J_{(u^*,v^*)} \right) \tilde{\mathbf{u}}. \tag{20}$$

To find solutions to this linear system of equations we first employ the method of separation of variables by looking for solutions of the form

$$\tilde{\mathbf{u}}(t, \mathbf{x}) = \phi(t) \tilde{\mathbf{w}}(\mathbf{x}). \tag{21}$$

This results in eigenvalue equations for $\tilde{\mathbf{w}}$ and $\phi(t)$ with accompanying boundary condition

$$\phi(t)' = \lambda \phi(t), \tag{22}$$

$$\lambda \tilde{\mathbf{w}} = D\nabla^2 \tilde{\mathbf{w}} + \gamma J_{(u^*,v^*)} \tilde{\mathbf{w}}, \qquad (\mathbf{n} \cdot \nabla)\tilde{\mathbf{w}} = 0 \quad \text{on } \partial\Omega. \tag{23}$$

Then (22) gives us that $\phi(t) = \phi(0) e^{\lambda t}$. To solve the spatially dependent equation (23) we use the fact that the eigenfunctions of the Laplacian, for both Dirichlet and Neumann boundary conditions on a general bounded domain $\Omega \subset \mathbb{R}^n$, form a countable (possibly infinite) orthonormal basis for the Hilbert space $L^2(\Omega)$. Thus we can express $\tilde{\mathbf{w}}$ as a linear combination of these eigenfunctions w_k

$$\tilde{\mathbf{w}}(\mathbf{x}) = \sum_k \mathbf{a}_k w_k(\mathbf{x}), \tag{24}$$

where w_k satisfies

$$\nabla^2 w_k = -k^2 w_k, \qquad (\mathbf{n}\cdot\nabla) w_k = 0 \quad \text{on } \partial\Omega. \tag{25}$$

If we now use this expansion of $\tilde{\mathbf{w}}$ and the fact that (20) is linear we get a solution-expansion of the form

$$\tilde{\mathbf{u}}(t,\mathbf{x}) = \sum_k \mathbf{a}_k e^{\lambda_k t} w_k(\mathbf{x}). \tag{26}$$

Substituting (21) in to (20), we arrive at an eigenvalue problem for λ_k

$$\lambda_k \mathbf{a}_k = \left(-Dk^2 + \gamma J_{(u^*,v^*)}\right) \mathbf{a}_k = \mathcal{A}\mathbf{a}_k, \tag{27}$$

which shows that the λ_k and $\mathbf{a}_k$ are eigenvalues and eigenvectors respectively of the matrix $\mathcal{A} = (-Dk^2 + J_{(u^*,v^*)})$. We are looking for a diffusion-driven unstable steady state and therefore (26) gives that we need at least one of the λ_k such that $\Re(\lambda_k) > 0$. In that case the perturbations around the steady state grow unbounded. If we again use the expression for eigenvalues of a 2×2-matrix we find that

$$\lambda_{k\pm} = \frac{1}{2}\left(\mathcal{T}_k \pm \sqrt{\mathcal{T}_k^2 - 4\mathcal{D}_k}\right), \tag{28}$$

$$\mathcal{T}_k = -k^2(1+d) + \gamma(f_u + g_v), \tag{29}$$

$$\mathcal{D}_k = dk^4 - \gamma(df_u + g_v)k^2 + \gamma^2(f_u g_v - f_v g_u). \tag{30}$$

For $\Re(\lambda_k) > 0$ we thus need either 1) $\mathcal{T}_k > 0$ or 2) $\sqrt{\mathcal{T}_k^2 - 4\mathcal{D}_k} > T_k$. However, since we already assumed (i) we know that $T_k < 0$ as γ, d are positive parameters. Therefore the condition required for Turing patterns is $\sqrt{\mathcal{T}_k^2 - 4\mathcal{D}_k} > T_k$ or $\mathcal{D}_k < 0$ for at least one k. Looking at (30), we can see that $\mathcal{D}_k$ is a quadratic polynomial in k^2. Using this information, we immediately spot a minimal requirement for $\mathcal{D}_k < 0$, namely $(df_u + g_v) > 0$, otherwise $\mathcal{D}_k$ has only positive elements since by (ii) $(f_u g_v - f_v g_u) > 0$. An interesting corollary of this is that we see that $d \neq 1$ must hold, so the chemicals must have different diffusion coefficients.
As $\mathcal{D}_k$ is a parabola in k^2, its minimum can be found to be

$$\mathcal{D}_{k\ min} = \frac{\gamma^2}{4d}\left(4d(f_u g_v - f_v g_u) - (df_u + g_v)^2\right), \tag{31}$$

which we need to be smaller than zero to get $\Re(\lambda_{k+}) > 0$. This gives a final set of conditions which are necessary for the creation of Turing patterns (but not sufficient as we shall see later on)

(iii) $df_u + g_v > 0$,
(iv) $(df_u + g_v)^2 - 4d(f_u g_v - f_v g_u) > 0$.

2.2. **Turing space.** Having derived the four necessary conditions (i),(ii),(iii),(iv) for Turing patterns based on linear analysis we can try to see what their implications are for our model of choice, the Schnakenberg model. As we have 4 free parameters a, b, γ, d it is interesting to see under what conditions they satisfy the Turing conditions and thus could give Turing patterns.

In order to do so, we look at the so-called Turing space in the parameter space, the region in the parameter space which satisfies the Turing conditions.

To carry out the analysis we take the explicit formulas for $f(u,v), g(u,v)$ and its partial derivatives for the Schnakenberg model to write out the explicit Turing conditions for the Schnakenberg model. To be able to formulate our conditions in an accessible manner, we set u^* as a parametric variable (which lies in the range $(0,\infty)$) and rewrite the Turing conditions in terms of the free parameters and this u^* variable using (14). Following Murray [11], we set out in this way to derive the boundary curves of the Turing space in the (a,b)-parameter space first. The first three Turing conditions become

(I) $f_u + g_v < 0 \implies 1 - \frac{2a}{u^*} - (u^*)^2 < 0 \implies a > \frac{u^*}{2}\left(1 - (u^*)^2\right)$,

(II) $f_u g_v - f_v g_u > 0 \implies (u^*)^2 > 0$,

(III) $df_u + g_v > 0 \implies d - (u^*)^2 - a\left(\frac{2d}{u^*}\right) > 0 \implies a < \frac{u^*}{2}\left(1 - \frac{(u^*)^2}{d}\right)$.

Note that the second one is trivially true and that since $d > 1$ the first and third condition do not contradict. For the last condition the amount of algebra starts to get cumbersome for the Schnakenberg model as we arrive at a quadratic equation in a

(IV) $(df_u + g_v)^2 - 4d(f_u g_v - f_v g_u) > 0 \implies c_1(d)a^2 - c_2(d)a + c_3(d) > 0$,

where we have

$$c_1(d) = 4d^2, \quad c_2(d) = 4du^*\left(d - (u^*)^2\right), \quad c_3(d) = (u^*)^2(d - (u^*)^2)^2 - 4d(u^*)^4. \tag{32}$$

Since this is a quadratic constraint it gives two possible conditions on a

$$a < \frac{c_2(d) - \sqrt{c_2(d)^2 - 4c_1(d)c_3(d)}}{2c_1(d)}, \quad a > \frac{c_2(d) + \sqrt{c_2(d)^2 - 4c_1(d)c_3(d)}}{2c_1(d)}, \tag{33}$$

which give after further inspection that one of the following two constraints must hold

$$a < \frac{u^*}{2}\left(1 - \frac{2u^*}{\sqrt{d}} - \frac{(u^*)^2}{d}\right), \quad a > \frac{u^*}{2}\left(1 + \frac{2u^*}{\sqrt{d}} - \frac{(u^*)^2}{d}\right). \tag{34}$$

The second of these two constraints is conflicting with (III) and thus cannot be satisfied. The first of (34) makes (III) superfluous and thus we end up with two boundary curves in the (a, b)-plane which bound the Turing space

(a) $a_{lower} > \frac{u^*}{2}\left(1 - (u^*)^2\right)$,

(b) $a_{upper} < \frac{u^*}{2}\left(1 - \frac{2u^*}{\sqrt{d}} - \frac{(u^*)^2}{d}\right)$.

Using u^* as a parameter going from 0 to ∞ and using the $b = u^* - a$ we can thus plot the bounding curves in the parameter space, see Figure 1. As the lower curve is independent of d, we can change the size of the Turing space by tuning d, and can even make it disappear for $1 < d < \tilde{d}_c$. To find $\tilde{d}_c$, one uses the fact that $\tilde{d}_c$ is the value for which upper curve goes through $(a, b) = (0, 1)$ to create the minimum size Turing space (just this point $(0, 1)$). The result is $\tilde{d}_c = 3 + 2\sqrt{2}$.

Given a particular pair (a, b) one can define a different critical diffusion ratio d_c, as the minimal value of d such that (a, b) lies in the Turing space, or patterns can form. It can again be found by finding d such that the upper curve passes through the point (a, b).

As a result, the function of (a, b) turns out to be more like a scaling for the problem, as it directly sets the steady states and gives a critical d_c for pattern formation, but the qualitatively behaviour of solutions does not depend strongly on (a, b) as numeric experiments showed. It is therefore interesting to look what happens if we set (a, b) to a certain fixed value and look at the effect of (γ, d).

2.2.1. *Mode selection.* So far we haven't been concerned with a crucial feature in our analysis, namely the form of the pattern that we expect to form in our model. Looking at the expansion of the perturbation (26) we note that the perturbations grow unbounded. This is a result of the omission of all non-linear terms, if we add those terms one expects to see finite amplitude solutions. However, the perturbations give a hint of what we can expect in the non-linear case. As the k-th mode-perturbation growth is governed by an exponential factor $e^{\lambda_k t}$ and these growth factors differ from mode to mode, we expect that the fastest growing mode will survive the initial perturbation phase and dominate the non-linear solution.

The cautious reader might have noticed that in deriving the Turing conditions we stated that the spatial eigenmodes form a countable set, hence the eigenvalues k must be discrete. In deriving the Turing conditions (iii),(iv) we only used the minimum value of $\mathcal{D}_k(k^2)$ and set it to smaller than zero. But if the spectrum k is discrete it might be that the k for which this minimum is

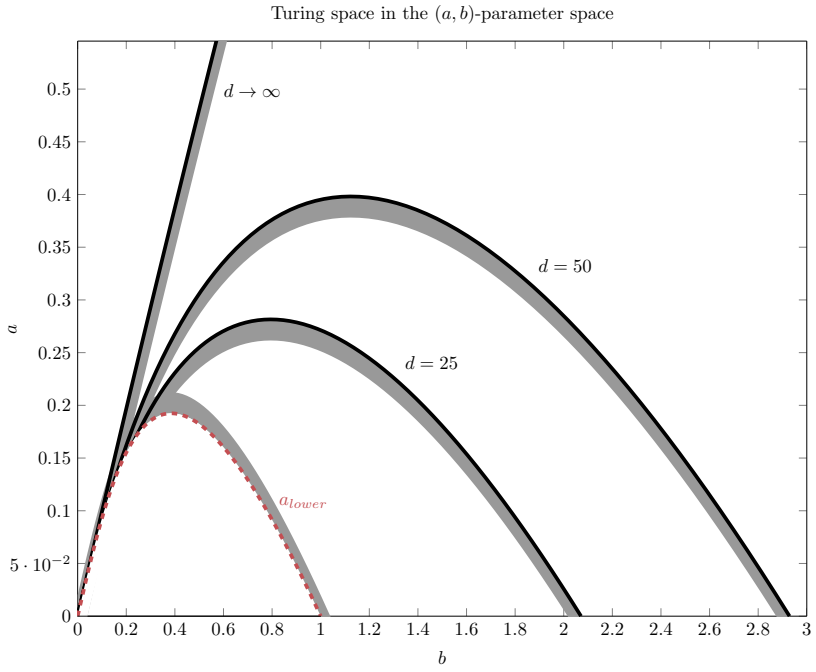

FIGURE 1. Turing space for parameters (a, b) of the Schnakenberg model for different values of diffusion ratio d. The bounding curves are given by (a),(b). The Turing space is bounded for finite values of $d > \tilde{d}_c = 3 + 2\sqrt{2}$ and grows by increasing d.

attained is not actually allowed. To account for this we take a close look at $\mathcal{D}_k$ and look for k such that $\mathcal{D}_k = 0$. This gives two k-values k_1, k_2 such that for $k^2 \in (k_1^2, k_2^2)$ $\mathcal{D}_k < 0$

$$k_1^2 = \frac{\gamma}{4d}\left((df_u + g_v) - \sqrt{(df_u + g_v)^2 - 4d(f_u g_v - f_v g_u)}\right), \tag{35}$$

$$k_2^2 = \frac{\gamma}{4d}\left((df_u + g_v) + \sqrt{(df_u + g_v)^2 - 4d(f_u g_v - f_v g_u)}\right). \tag{36}$$

To form patterns we thus need at least one of the eigenvalues from the discrete spectrum to lie within this interval of instability. To proceed further we need to know the actual values of k and thus we analyse the one-dimensional case where we take the unit domain $\Omega = [0, 1]$ to which all other one-dimensional domains can be rescaled. Note that the approach taken here can be equally applied to different Ω as long as there is an expression for the eigenvalues of the k-th mode, either analytical or numerical. The eigenvalue/eigenfunction pairs in the aforementioned case are known to be of the form

$$w_k(x) = \cos(kx), \qquad k = m\pi. \tag{37}$$

Knowing k we can find the region in (γ, d)-space for which the mode is excitable by finding the marginal stability curves, i.e. the curves for which $\lambda_k = 0$ using (28), see Figure 2a. For each given k these curves divide the parameter space in a stable region, where the perturbation grows, and unstable region, where it decays. The result can be seen in Figure 2b.

Since there exist large parts of the excitable space that overlap for different modes it is interesting to see which mode dominates at a point (γ, d) and thus gets selected by letting time increase, hence the name mode selection. Therefore we construct a predicted domination area for the k-th mode following Arcuri et al. [1], who analysed the mode selection process in the Thomas model in detail.

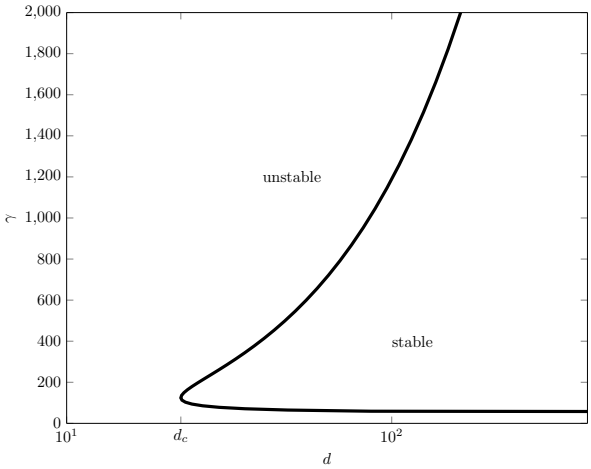

(A) Marginal stability curve for the 2nd mode dividing the parameter space in two parts depending on the stability of the mode.

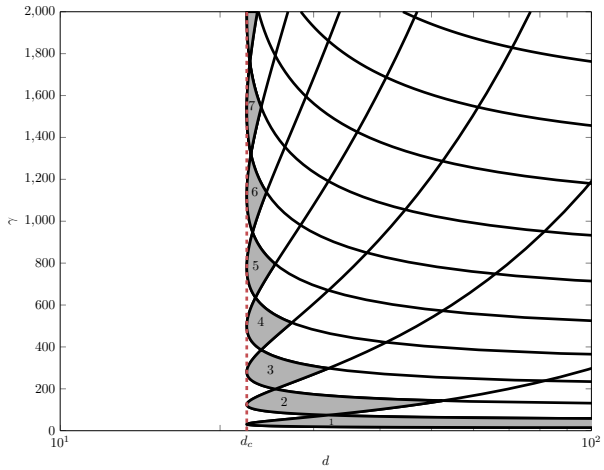

(B) Combination of the marginal stability curves of the first 8 modes. Plotted in grey are areas in which only one mode is stable.

FIGURE 2. Building up the Turing space in (γ, d)-parameter space of the Schnakenberg model for $(a, b) = (0.2, 1.3)$ on $\Omega = [0, 1]$ by use of the marginal stability curves for the first 8 modes.

This area is defined to be the region in which k has the largest growing rate λ_k. In the grey areas in Figure 2b only one possible mode is excitable and thus these regions are trivially categorised. To determine the boundaries of the domination region for the k-th mode we use that fact that on the bounding curves it must hold that the growth rates of adjoining modes are equal, i.e. $\lambda_k = \lambda_{k+1}$. This finally divides the parameter space in a Turing space for the different modes based on linear analysis, see Figure 3. Note that the linear theory without considering the modes predicts patterns in the region where $d > d_c$, but taking into account discrete modes gives patches where actually no mode is excitable. The values of (a, b) only change the picture quantitatively confirming our earlier comment on the effect of (a, b) as merely scaling variables.

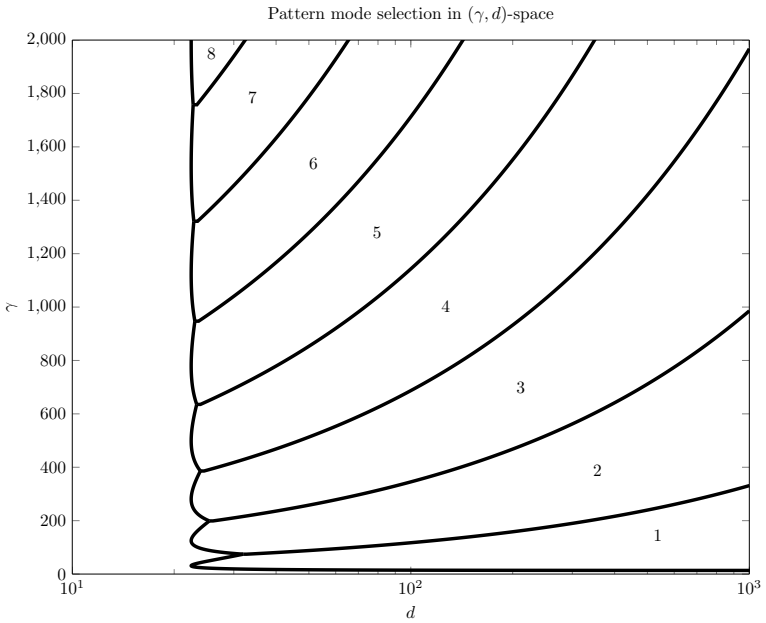

FIGURE 3. Turing space in (γ, d)-parameter space of the Schnakenberg model for $(a, b) = (0.2, 1.3)$ on $\Omega = [0, 1]$. Indicated are the fastest growing pattern modes based on linear stability analysis. The fastest growing mode is the expected candidate to survive and dominate in the non-linear regime of the model.

2.2.2. *Fourier decomposition.* As a result of the non-linear interactions the final patterns are expected to have a finite amplitude, which is a minimal requirement for the model as well since the model has to be chemically plausible. Taking this into account one might be tempted to state as a final solution

$$\mathbf{u} = \mathbf{u}^* + A(t)\mathbf{a}_k w_k(\mathbf{x}), \tag{38}$$

where $A(t)$ is some amplitude function which should go to a constant as $t \to \infty$. Even though this might work for a linear equation, non-linear equations cause the excitation of higher modes. For the case we considered earlier $\Omega = [0, 1]$ with Neumann boundary this can be seen by noting that for example quadratic terms give

$$\cos(kx)^2 = \frac{1}{2}\left(1 + \cos(2kx)\right). \tag{39}$$

Therefore higher modes can get into the solution, depending on the type of non-linearity, e.g. quadratic or cubic. Thus we need to adapt our expansion of the solution to involve higher modes as well

$$\mathbf{u} = \mathbf{u}^* + \sum_{i=1}^{\infty} A_i(t)\mathbf{a}_{ik} w_{ik}(\mathbf{x}). \tag{40}$$

To find the contributions of the higher modes in the solution we can calculate the coefficients by using the fact that $\{w_n(\mathbf{x})\}$ forms an orthonormal basis

$$A_m(t)\mathbf{a}_m = \int_\Omega \mathbf{u} w_m d\Omega. \tag{41}$$

If we started out from a random initial condition such as white noise, thus containing all the different modes, we would in general expect higher order modes to have smaller amplitudes compared

to mode k. This is due to the fact that in the initial phase, when the perturbations around the steady state are still small, the system is well described by the linearised system (20). This system predicts that the higher modes have a strong decay rate λ_{ik} and thus will tend to zero. It is only because of the non-linear terms for large enough $\mathbf{u}$ that the higher order multiples of the k-th mode enter the solution. This imposes challenges for the numerical simulation of these type of models as we shall see in the next part.

3. Numerical analysis

In our approach to Turing conditions we heavily relied on the small perturbation assumption, thus neglecting all the non-linear effects. As the equations are non-linear in nature we need a different angle to conclude anything about the long-term final pattern formation and probably the most used strategy to study the non-linear regime is the use of numerical methods.

3.1. **PDE time stepping.**

To solve (8) numerically we use a standard method in solving PDE's, the method of lines (MOL) [8]. The basic ingredient is that we convert the PDE to a system of ODEs by first discretizing the PDE in the spatial direction. This replaces the continuous $\mathbf{c}(\mathbf{x},t)$ by a vector $\mathbf{C}(t) = (\mathbf{C}_j(t))_{j=1}^m$ defined on a discrete grid with m points $\{\mathbf{x}_j\}_{j=1}^m$, such that $\mathbf{C}_j(t) \approx \mathbf{c}(\mathbf{x}_j,t)$. By discretizing in the spatial direction we replace the Laplacian operator in (8) with an operator $\mathbf{F}_1(t,\mathbf{C}(t))$ and the reaction terms are governed by $\mathbf{F}_2(t,\mathbf{C}(t))$

$$\frac{d}{dt}\mathbf{C}(t) = \mathbf{F}_1(t,\mathbf{C}(t)) + \mathbf{F}_2(t,\mathbf{C}(t)). \tag{42}$$

The resulting ODE-system is then solved along lines of constant position, hence the method of lines, using a suitable ODE integration scheme. As one can already anticipate, there are two crucial ingredients in deriving the final method, namely the type of spatial discretisation and the ODE integration scheme, which we thus describe next.

3.1.1. *Spatial discretisation.*

The main goal of using a spatial discretisation is to replace the Laplacian operator. The result is often a matrix D_2 such that $(D_2\mathbf{C}(t))_j \approx \nabla^2\mathbf{c}(\mathbf{x}_j,t)$.

A standard approach would be to use finite difference methods to approximate the Laplacian operator on a uniform grid [8], resulting in a sparse matrix D_2. The convergence rate of these methods is of the form $\mathcal{O}(N^{-m})$ where m is a fixed number depicting the order of the finite difference method and N the number of gridpoints.

For this paper we are interested in the spatial heterogeneous pattern that forms after finite time and especially its decomposition in Fourier modes. In order to calculate the coefficients of the Fourier modes we need to calculate (41), but since we discretise the spatial direction we can only hope to approximate the integral using the values on the spatial grid $\{\mathbf{x}_j\}_{j=1}^m$. One of the main disadvantages of using the finite difference method is the fact that it can severely suffer from an effect called aliasing. Since we use an equispaced finite grid, only a fixed number of modes can be represented on the grid. The modes have to lie within a range given by the Nyquist limit. In the one-dimensional case, with a spacing h between the gridpoints, i.e. $x_j = jh$, we find that $k \in [\frac{-\pi}{h}, \frac{\pi}{h}]$ is the allowed interval. All the higher mode components get mapped to modes within the interval set by the Nyquist limits and thus they pollute the solution components of the lower modes. One way to overcome this problem would be to increase the number of points and thus decrease h. This would give a wider bandwidth of allowed modes. However, the approximation of the coefficients would still need to be done by a trapezoidal integration or similar Newton-Cotes formulas, which is not a particular accurate numerical quadrature.

This forms one of the motivations for the use of a spectral method [14]. As we wish to use non-periodic boundary conditions we can employ as basis functions the Chebyshev polynomials. Since this method uses an global approximation scheme on a non-uniform Chebyshev grid the method is expected to give spectral accuracy, i.e. convergence at a rate $\mathcal{O}(N^{-m})$ for every $m \geq 0$ with N the number of gridpoints, which is much better than the rate observed for finite difference

methods. So we expect to be able to use less gridpoints. The trade-off however using spectral methods is that D_2 is not sparse, but dense, and thus the calculations with it tend to take longer. To make the spectral method even more favourable, it allows one to use a better quadrature rule to approximate the integrals. Since the concentrations of the chemicals are known on the Chebyshev points we can use the Clenshaw-Curtis quadrature [14], which will give us more accuracy using less gridpoints in determining the Fourier coefficients.

3.1.2. *IMEX methods.* Recall that the result of the spatial discretisation was a system of ODEs containing two different operators $\mathbf{F}_1, \mathbf{F}_2$ (42). Both terms have a distinct nature as diffusion makes $\mathbf{F}_1$ a stiff term whereas the reactions can be regarded as non-stiff. This imposes severe constraints on step-size and mesh-size of the scheme if we were to use an explicit method. On the other hand, using a fully implicit method would lead us with no other option than to use Newton iterations each time step to cope with the non-linear reaction terms, which is very likely to seriously increase the computational time.

A compromise between the fully explicit or implicit method makes use of the exact splitting of the problem as in (42) and treats the non-stiff terms explicitly whereas the stiff terms are integrated implicitly in time. This class of schemes are known as implicit-explicit methods (IMEX) [8]. Three IMEX schemes based on Ruuth [12] were used to integrate (42)

$$\frac{3}{2}\mathbf{C}^{n+1} - 2\mathbf{C}^n + \frac{1}{2}\mathbf{C}^{n-1} = \Delta t \mathbf{F}_1^{n+1} + \Delta t \left(2\mathbf{F}_2^n - \mathbf{F}_2^{n-1}\right), \quad \textit{IMEX-BDF2} \tag{43}$$

$$\mathbf{C}^{n+1} - \mathbf{C}^n = \frac{\Delta t}{2}\left(\mathbf{F}_1^{n+1} + \mathbf{F}_1^n\right) + \frac{\Delta t}{2}\left(3\mathbf{F}_2^n - \mathbf{F}_1^{n-1}\right), \quad \textit{IMEX-Euler} \tag{44}$$

$$\mathbf{C}^{n+1} - \mathbf{C}^n = \Delta t \mathbf{F}_1^{n+1} + \Delta t \left(2\mathbf{F}_2^n + \mathbf{F}_2^{n-1}\right). \quad \textit{IMEX-CNAB} \tag{45}$$

IMEX-BDF2 (backward differentiation) and IMEX-CNAB (Crank-Nicolson-Adams-Bashfort) are two-step methods and are second order, whereas the IMEX-Euler method is first order and a one-step method. As aliasing and the correct representation of Fourier modes are of interest for this paper, we noted in the simulation of the Schnakenberg that the IMEX-CNAB method, although second order in time, performed worse than the other two methods. This can be understood by looking at the damping factor for the modes introduced by the schemes. As we want to correctly describe the dominant modes, which are mostly low modes, it would be advantageous to have a numerical scheme with good damping of the high modes, thereby decreasing the risk of aliasing. As found by Ascher et al. [2], the IMEX-CNAB scheme is a weakly damping scheme and thus very prone to show aliasing effects. The IMEX-Euler and IMEX-BDF2 scheme on the other hand are strongly damping and are more robust for our purposes, which is what we saw in simulations as well. The practical damping properties of the schemes were thus found to be consistent with Ruuth [12]. As the calculation of the results of IMEX-Euler and IMEX-BDF2 were found to take roughly the same time and the IMEX-BDF2 method is second order, the main results in this paper were calculated using the latter method.

As a final note on the time step-size, we need to take the time step initially small enough for the decay of the high-frequency modes to take effect as predicted by the linear system. If the initial time step is taken too big, the high modes might not be removed and thus form spurious solutions. The fact that the two strongly damping IMEX schemes have a natural filter against aliasing would suggest that an adaptive step-size after the initial phase could be applicable and thus reduce computation time. This was however outside the scope of this paper.

3.2. **Numerical Turing space.** A typical result from the numerical simulations using the IMEX-BDF2 method can be seen in Figure 4. The simulation agrees with the predictions from the linear theory. However, the presence of the higher modes, as can be seen in it's Fourier decomposition in Figure 4b, was not anticipated by linear theory. It can be seen from the Fourier decomposition

that the solution is indeed of the form (40) with $k = 2$, as it turns out that the value of $|a_0|$ exactly corresponds with the steady state u^*.

Linear theory however has its limits as can be seen from a great number of simulation which give modes which are not expected to dominate, see Figure 5. The mode that is excited has a growth rate which is bigger than zero, so it could be excited, linear theory predicts nevertheless that there should be a mode with a bigger growth rate. Here we see that the formation of the pattern appears to be sensitive to the initial conditions, as we get different results if we simulate with the same parameters but different random initial conditions.

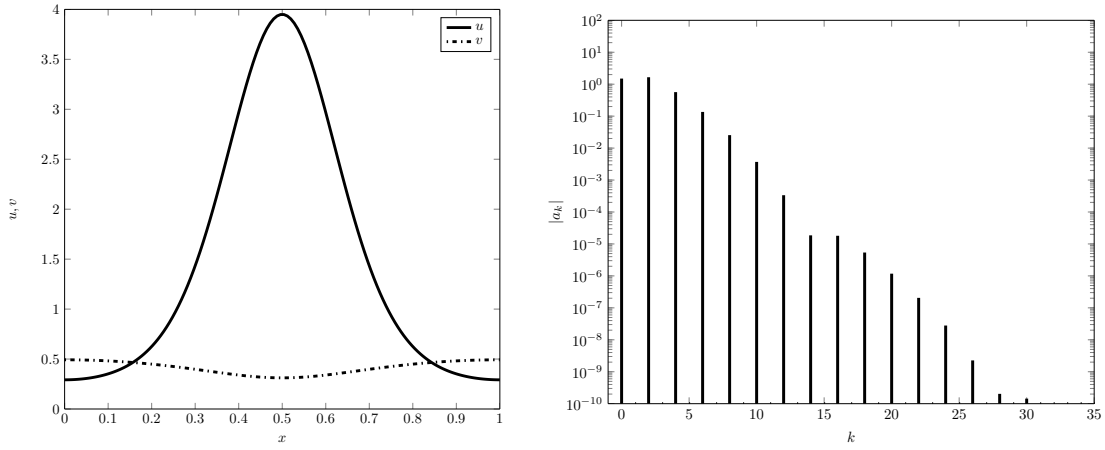

(A) Solution plot for u, v.

(B) Amplitude of the Fourier coefficients for the solution component u in Figure 4a.

FIGURE 4. Numerical solution of the Schnakenberg model for $(a, b, \gamma, d) = (0.2, 1.3, 220, 119)$ on $\Omega = [0, 1]$. From the Fourier coefficients it can be observed that the pattern is mainly described by the second mode as predicted by linear theory, see Figure 3.

We can summarise the result of many numerical simulations for different parameter values in the (γ, d) domain by plotting the final mode in the (γ, d)-space and thus create a numerical equivalent to Figure 3. An example of such a result is depicted in Figure 6 and has some striking features. First of all the linear theory seems to work quite well near the critical value d_c as was expected. However, the plot suggests that there are regions where the linear theory predicts a steady homogeneous solution, but the numerics show that there actually exists a stable heterogeneous solution. This suggests that the homogeneous solution is in some kind of metastable state. Further numerical investigation seems to indicate that the amplitude of the resulting subcritical instabilities are very small, see Figure 7, and that they are not numerical artefacts, as they do not vanish if we change the mesh or step-size or the integration method. Of course the biological importance of these subcritical instabilities is small if they have an amplitude which makes it nearly indistinguishable from the steady state. In that way they would never be able to generate a pre-pattern, as the model validity has to be questioned for such small differences. However, the possible existence of a subcritical Turing instability could of course be of mathematical interest.

Other remarks can be made upon inspection of Figure 6. For values away from d_c it seems that the modes mix, in the sense that it is hard to distinguish hard boundaries between domination regions (this effect can be seen more profoundly in appendix A). It looks like the initial conditions highly influence the final pattern which makes one wonder about the robustness of the pattern formation in this model. If a slight perturbation in the (noisy) initial conditions gives a different

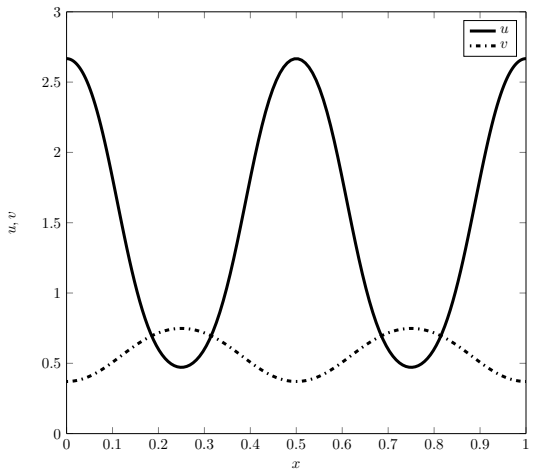

(A) Solution plot for u, v.

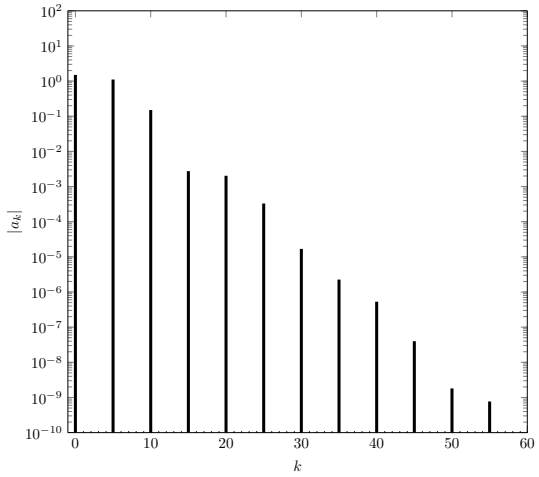

(B) Amplitude of the Fourier coefficients for the solution component u in Figure 5a.

FIGURE 5. Numerical solution of the Schnakenberg model for $(a, b, \gamma, d) = (0.2, 1.3, 920, 40)$ on $\Omega = [0, 1]$. Although quite close to d_c, the final pattern is in the 4-th mode instead of the 5-th mode which linear theory predicted, see Figure 3.

pattern, this model is unable to explain the great coherence in the patterns of different individuals of the same species.

4. Discussion and conclusions

In this paper we derived the Turing conditions for a diffusion-driven instability. We showed how these conditions in the case of the Schnakenberg model give rise to a domain in parameter space where patterns can form, the Turing space. Already in the one-dimensional case non-trivial behaviour can be observed in this model.

Numerical simulations suggest the existence of a subcritical Turing instability in the Schnakenberg model. A possible way to study this phenomena in more detail is by setting out a weakly non-linear analysis, which is unfortunately outside the scope of this paper. Since the diffusion close to the critical value can be written as $d = d_c(1 + \varepsilon)$, where ε is a small parameter, we can use an expansion in this small parameter for the weakly non-linear analysis. This way one can set out to derive a Landau equation for the amplitudes of the modes when close to the critical value. If such an equation can be found, the stability analysis of this amplitude equation could show the existence of a subcritical instability, such as in Wollkind et al. [16].

Another interesting approach to the numerical solution of the reaction diffusion equations could be to consider a Fourier spectral method. This way one can directly keep track of the Fourier modes, as we compute the solution by decomposing it onto its Fourier modes. The downside of the Fourier spectral method in this case is that it is only applicable to periodic domains, which doesn't seem to be the case for the common case of a Neumann boundary condition. Note however, that we can view the Neumann boundary value problem as a periodic problem on a domain twice the size by reflecting the original domain in one of the endpoints. Therefore by introducing a grid of twice the original size with periodic boundary conditions one could use a Fourier spectral method, which can result in an enormous speed-up, see Kassam et al. [9], if used in combination with good de-aliasing measures, e.g. Boyd [3].

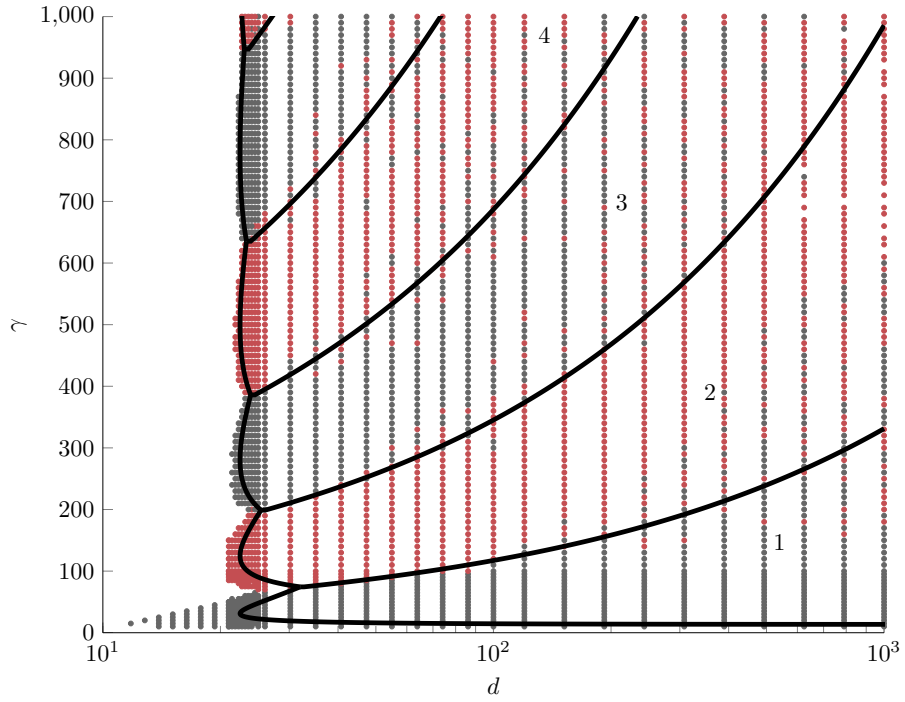

FIGURE 6. Numerical realization of the Turing space in (γ, d)-parameter space of the Schnakenberg model for $(a, b) = (0.2, 1.3)$ on $\Omega = [0, 1]$. Indicated with dots are the most dominant pattern modes in the final heterogeneous patterns, the colors indicate which mode, • for modes 2,4,6 and • for modes 1,3,5. In black overlay is the predicted Turing Space based on linear theory, see Figure 3.

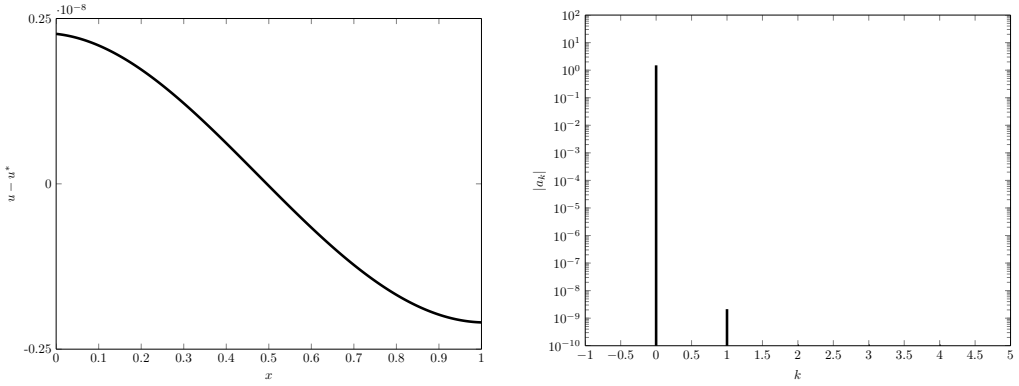

(A) Solution plot for $u - u^*$.

(B) Amplitude of the Fourier coefficients for the solution component u in Figure 5a.

FIGURE 7. Numerical solution of the Schnakenberg model for $(a, b, \gamma, d) = (0.2, 1.3, 35, 20)$ on $\Omega = [0, 1]$. For a subcritical value of d it appears that the final solution is not the steady state as is predicted by linear theory predicted. Instead we get a very small amplitude 1-st mode heteregenous state.

From the numerical simulations it could be observed that the Neumann boundary conditions problem seems to become highly sensitive to initial conditions for higher mode numbers. This damages the robustness of the mode selection of the specific model. The numerically computed Turing domains, as we can see in appendix A, are quite large so a small change in parameters (γ, d), if not in the neighbourhood of a marginal stability curve doesn't change the situation much. The problem of sensitivity lies as we observed in values close to the marginal stability curves which we derived in the linear theory. Methods to improve the robustness of pattern formation have been proposed in the literature, such as different boundary conditions by Arcuri et al. [1], or growth of the domain in time, e.g. by Crampin et al. [4].

Another obvious extension of the work presented in this paper is the step to two or even three dimensional pattern formation. The possibility of a degeneracy of eigenvalues makes it harder to predict the pattern based on linear theory, but weakly non-linear theory is in some cases. Furthermore could the methods presented here be applied to different models, like the ones mentioned in the introduction, as most of the theoretical results of the first chapter can equally well be transferred to different models.

Appendix A. Numerically generated Turing space

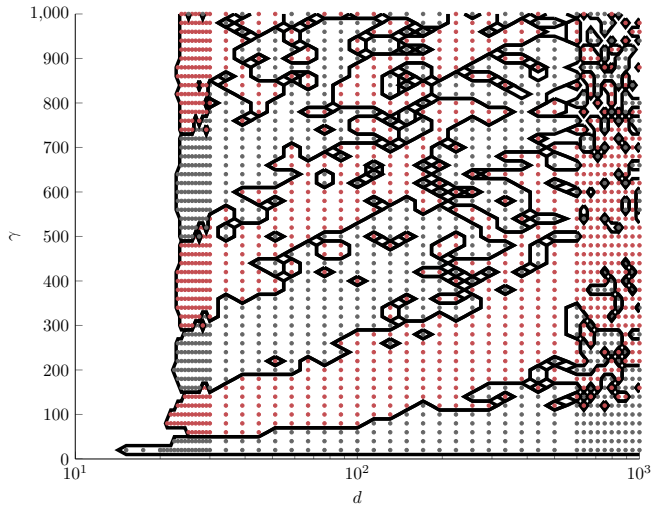

(A) $(a, b) = (0, 2)$.

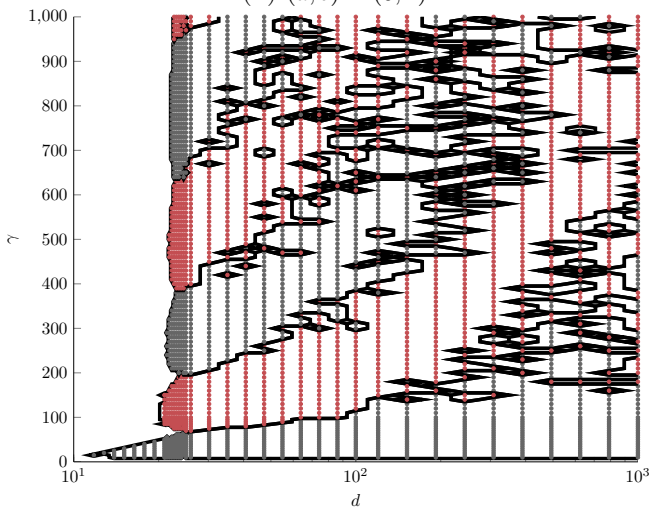

(B) $(a, b) = (0.2, 1.3)$.

Figure 8. Numerical realization of Turing spaces in (γ, d)-parameter space of the Schnakenberg model on $\Omega = [0, 1]$. Indicated with dots are the most dominant pattern modes in the final heterogeneous patterns, the colors indicate which mode, • for modes 2,4,6 and • for modes 1,3,5.

To construct the numerical Turing Spaces, we integrated the Schnakenberg model for each dot in the parameter space starting with random initial conditions centred at the steady state. Then using the numerical quadrature we could approximate the Fourier coefficients and find the largest component among them. This gave the classification into different modes of the parameter space.

The values of (a, b) do not change the qualitative behaviour of the Turing space as can be observed. The presence of a subcritical instability for the lowest two modes can be seen as well.

Appendix B. Gallery of one-dimensional Schnakenberg patterns

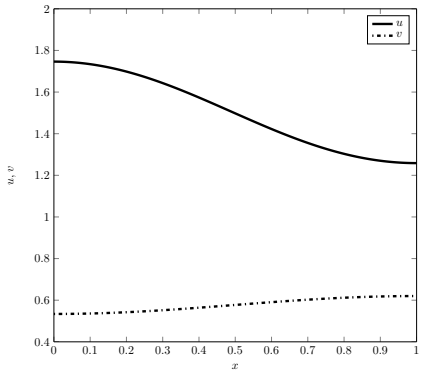

(A) $(\gamma, d) = (30, 40), k = \pi$.

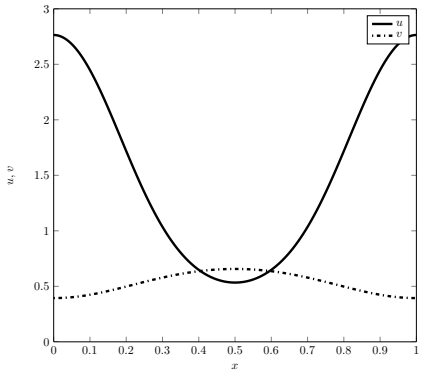

(B) $(\gamma, d) = (140, 40), k = 2\pi$.

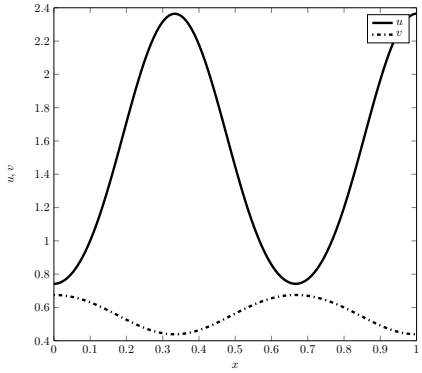

(C) $(\gamma, d) = (250, 40), k = 3\pi$.

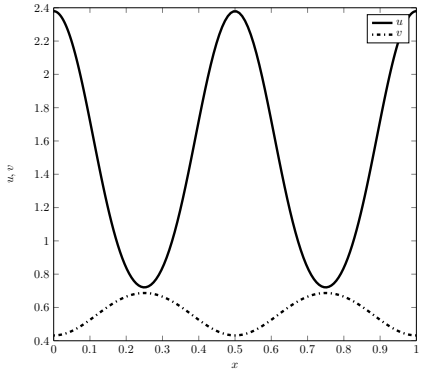

(D) $(\gamma, d) = (490, 40), k = 4\pi$.

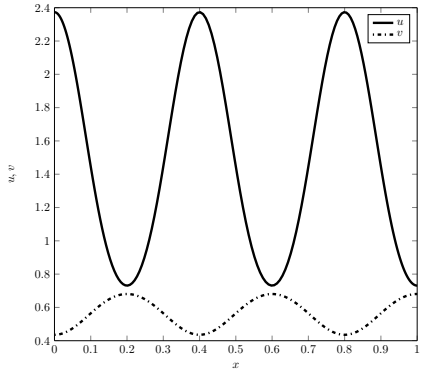

(E) $(\gamma, d) = (820, 40), k = 5\pi$.

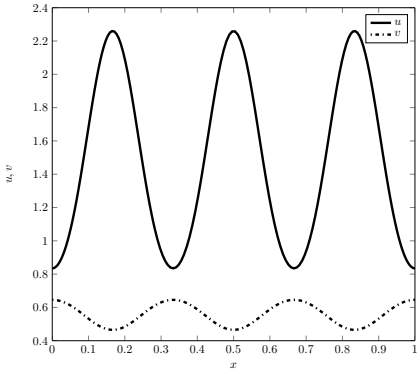

(F) $(\gamma, d) = (1000, 40), k = 6\pi$.

FIGURE 9. Different modes for $(a, b) = (0.2, 1.3)$.

References

1. Arcuri, P. & Murray, J. Pattern sensitivity to boundary and initial conditions in reaction-diffusion models. *Journal of mathematical biology* **24,** 141–65 (1986).
2. Ascher, U. M., Ruuth, S. J., Brian & Wetton, B. T. R. Implicit-Explicit Methods For Time-Dependent PDEs. *SIAM J. Numer. Anal* **32,** 797–823 (1997).
3. Boyd, J. P. *Chebyshev and Fourier Spectral Methods: Second Revised Edition* (Courier Corporation, 2001).
4. Crampin, E, Gaffney, E & Maini, P. K. Reaction and Diffusion on Growing Domains: Scenarios for Robust Pattern Formation. *Bulletin of Mathematical Biology* **61,** 1093–1120 (1999).
5. Fitzhugh, R. Impulses and Physiological States in Theoretical Models of Nerve Membrane. *Biophysical journal* **1,** 445–66 (1961).
6. Gierer, A. & Meinhardt, H. A theory of biological pattern formation. *Kybernetik* **12,** 30–39 (1972).
7. Gray, P. & Scott, S. Autocatalytic reactions in the isothermal, continuous stirred tank reactor. *Chemical Engineering Science* **39,** 1087–1097 (1984).
8. Hundsdorfer, W. & Verwer, J. G. *Numerical Solution of Time-Dependent Advection-Diffusion-Reaction Equations* (Springer Science & Business Media, 2003).
9. Kassam, A.-K. & Trefethen, L. N. Fourth-Order Time-Stepping for Stiff PDEs. *SIAM Journal on Scientific Computing* **26,** 1214–1233 (2005).
10. Murray, J. *Mathematical Biology II: Spatial Models and Biomedical Applications* 3th (ed Murray, J. D.) (Springer-Verlag, New York, 2003).
11. Murray, J. Parameter space for turing instability in reaction diffusion mechanisms: A comparison of models. *Journal of Theoretical Biology* **98,** 143–163 (1982).
12. Ruuth, S. J. Implicit-explicit methods for reaction-diffusion problems in pattern formation. *Journal of Mathematical Biology* **34,** 148–176 (1995).
13. Schnakenberg, J. Simple chemical reaction systems with limit cycle behaviour. *Journal of Theoretical Biology* **81,** 389–400 (1979).
14. Trefethen, L. N. *Spectral Methods in MATLAB* (Society for Industrial and Applied Mathematics, 2000).
15. Turing, A. The chemical basis of morphogenesis. *Philosophical Transactions of the Royal Society of London. Series B, Biological Sciences* **237,** 37–72 (1952).
16. Wollkind, D. J., Manoranjan, V. S. & Zhang, L. Weakly Nonlinear Stability Analyses of Prototype Reaction-Diffusion Model Equations. *SIAM Review* **36,** 176–214 (1994).
17. Wolpert, L. Positional information and the spatial pattern of cellular differentiation. *Journal of Theoretical Biology* **25,** 1–47 (1969).